A framework to predict the airborne noise inside railway vehicles with application to rolling noise

Hui Li[1], David Thompson[1], Giacomo Squicciarini[1], Xiaowan Liu[1], Martin Rissmann[2], Pascal Bouvet[2], Francisco D. Denia[3], Luis Baeza[3], Julián Martín Jarillo[4], Juan Moreno García-Loygorri[4]

[1]Institute of Sound and Vibration Research, University of Southampton, Southampton SO17 1BJ, United Kingdom
[2]Vibratec, Chemin du Petit Bois BP 36, F-69131 Ecully Cedex, France
[3]Centro de Investigación en Ingeniería Mecánica, Universitat Politècnica de València, Camino de Vera s/n, 46022 Valencia, Spain
[4] Servicio de Ingeniería de Material Móvil, Área de Ingeniería, Metro de Madrid S.A., Calle del Néctar 44, 28022 Madrid, Spain

Abstract

A framework is described for predicting the airborne noise inside railway vehicles which is applied to rolling noise sources. Statistical energy analysis (SEA) is used to predict the interior noise by subdividing the train cabin into several subsystems. The dissipation loss factors are obtained from the measured reverberation time in the train cabin. The power input to the interior SEA model is obtained from the external noise sources by multiplying the incident sound power on the external surfaces with measured transmission coefficients of the train floor and sidewalls. The sound power incident on the train floor is calculated by using an equivalent source model for the wheels and track together with an SEA model of the region below the floor. The incident sound power on the sides is obtained by using a waveguide boundary element (2.5D BE) method. The procedure is applied to a Spanish metro train vehicle running in the open field for which rolling noise is the main external noise source. The procedure is verified by field measurements of sound pressure beneath the carriage, on the sidewalls and inside the vehicle. The sensitivity of the results to changes in interior absorption is also studied, including the effect of passengers.

Key works: Railway vehicle, interior noise, statistical energy analysis, 2.5D boundary element method, rolling noise

1 Introduction

Various complex sources contribute to the interior noise in railway vehicles. The mechanisms by which noise generated by these sources reaches the passenger in a train cabin were discussed

in refs. [1, 2]. Rolling noise is generally the most important source for speeds below 300 km/h, whereas aerodynamic noise becomes important above this speed [3]. Rolling noise consists of components radiated by the wheels, the rails and the sleepers and it can be transmitted to the interior space through both structure-borne and airborne paths [3, 4]. Suspension springs, dampers and connecting rods constitute paths for structural vibration which can lead to structure-borne sound radiation inside the vehicle. Besides, the turbulent boundary layer and vortex shedding caused by train components will also generate structure-borne noise [5], as well as aerodynamic noise which is transmitted by airborne paths. Sound waves impinging on the external surfaces of the train can be transmitted to the interior by airborne transmission through the train floor and sidewalls, which often consist of relatively light extruded panels. Doors, windows and gangways may also form paths for significant airborne noise transmission. Furthermore, additional equipment, such as air conditioning and ventilation systems, motors, gearboxes, electrical converters and compressors, can be located beneath or inside the train and contribute to a complicated acoustic environment in railway vehicles. Due to the complex noise sources associated with railway vehicles, and their specific designs, the distribution of noise levels inside railway vehicles along the longitudinal direction can vary in a wide range. Guo. et al. [6] measured the noise levels inside a metro vehicle running in a tunnel. Their measured results show differences of up to 8 dB(A) at different locations in the carriage, with the highest levels in the gangway region and the lowest levels in the centre of the car. Yan et al. [7] considered a metro vehicle on a viaduct and the measured data show only about 1 dB(A) difference in sound pressure levels at the end and in the middle of the metro carriage, although they did not include the gangway region.

Modelling approaches that are both highly efficient and sufficiently accurate are required to predict the interior noise, especially at the early design stage. Established methodologies for this purpose include the finite element/boundary element (FE/BE) method at low frequency [8], statistical energy analysis (SEA) at high frequency and a hybrid FE-SEA approach at medium frequency. Shorter et al. [9] provided a qualitative definition of the mid-frequency problem and suggested that a statistical description of the local dynamic properties of a system is an essential element of any mid-frequency prediction method. A hybrid approach to the mid-frequency problem was described in [9] which employs a statistical description of the local modal properties of various subsystems. Ji et al. [10] reviewed the vibro-acoustic modelling of extruded aluminium train floor structures with the purpose of predicting mid-frequency vibro-acoustic responses of such stiffened panel structures to an acceptable accuracy at a reasonable

computational cost, which can be helpful for interior noise modelling in the mid-frequency range.

SEA has the reputation of solving problems associated with large structures and high frequencies with little computational effort. The use of the SEA method to predict noise inside a railway vehicle has advantages because the train cabin is relatively large and, even at relatively low frequency, there are many acoustic modes involved in the response. 'Weak coupling' conditions can be fulfilled in the SEA sense, which requires there to be predominantly local modes in each subsystem [11]. The SEA method has been used by many researchers to investigate the sound distribution in the train cabin. For instance, De Meester et al. [12] employed an experimental SEA (ESEA) to predict the noise inside a high-speed train carriage. Stegemann [13] developed a vibro-acoustic model for a metro rail car using SEA, which included the train structure, noise control treatments and acoustic spaces surrounding the vehicle. Sadri et al. [14] used a predictive SEA model to calculate the noise inside a passenger vehicle. In their model a combination of the classical SEA method and a Bayesian technique was used to overcome the uncertainty caused by the presence of possible strong coupling between subsystems and the lack of diffuseness in the train cabin. Forssén et al. [15] employed a conventional SEA model to predict the noise inside a 1:5 scale model railway vehicle, but within each subsystem the spatial decay was adjusted using formulae for the sound decay in corridors [16]. The sound pressure levels predicted in the train cabin at various points were in reasonable agreement with measured results at most frequencies. Zheng et al. [17, 18] and Dai et al. [19] proposed a statistical energy flow method to predict the full spectrum sound inside a railway vehicle. Their models included rolling noise and aerodynamic noise. The predictions had good agreement with measured data with differences less than 3 dB in terms of overall sound pressure levels. Zhang et al. [20] used an SEA model to study the train interior noise and analysed the contributions from factors such as the vibration of sidewalls, the noise source in the bogie area, and the transmission loss of the floor. The results from their SEA model were in good agreement with experimental measurements. According to their investigations, they proposed a comprehensive acoustic design procedure to control the interior noise in trains [21].

However, one of the main challenges of applying the SEA method for prediction of interior noise is to evaluate the input power. Forssén et al. [15] considered only noise sources located inside the train while the most important ones located outside were not considered. In the work

of Zheng et al. [17] and Dai et al. [19], the exterior sound field was calculated using full-scale three dimensional models, which require large computation times. Bistagnino et al. [22] adopted a Fast Multipole BE method and a Beam-tracing technique to predict the sound pressure on the train walls due to rolling noise. A reasonable agreement with measurements was achieved and the numerical techniques adopted in their work reduced the computational time and memory usage compared with the traditional BE method; in their model, however, it is not easy to consider the complicated sources outside the train. Kohrs et al. [23] compared different approaches and methods, including BEM, ray tracing and SEA, to calculate the pressure field around the car body for either artificial sources or real operation in free field and in tunnel. Acceptable accuracy was achieved although various simplifications and assumptions had to be made and there were uncertainties in the various parameters involved.

Based on the existing research in the literature and its limitations, this paper provides a modelling approach to predict the noise inside a train cabin when running in open field. Bouvet et al. [4] reviewed the relative contributions of the airborne and structure-borne paths to the noise inside railway vehicles, and pointed out that generally the airborne path is dominant in the middle and high frequency range and the structure-borne only has significant effect at low frequency, although this depends on the particular design of the train. This work, therefore, focusses on the airborne transmission path. The approach is outlined assuming that the most significant source is rolling noise but could also be used for other sources. The sound powers incident on the train floor and on the sides are treated separately. Because of the complex geometry below the train floor, an SEA model [24] is preferred to traditional FE/BE methods or the ray tracing method [22] for predicting the sound power incident on the train floor. The sound incident on the train sides is mainly caused by diffraction. In this case a wavenumber domain boundary element (2.5D BE) method [25] is used to evaluate the sound power incident on the sidewalls. The sound power transmitted into the train cabin is then obtained by multiplying the incident powers with the transmission coefficients of the train floor and sidewalls. These could be obtained from a prediction model but in the present example they are obtained experimentally. The noise inside the vehicle is then predicted by means of a separate SEA model created for the interior space.

In the remainder of the paper Section 2 introduces the SEA model for the prediction of noise inside a railway vehicle while Section 3 explains how the power input to the SEA model is determined. The procedure is applied to predict the noise inside a metro vehicle in Section 4

and the results are compared with measured data in Section 5. A short discussion about the assumptions in this framework is given in Section 6 and this is followed by the conclusions in Section 7.

2 SEA model for prediction of railway vehicle interior noise

In the use of an SEA model, the train cabin needs to be divided into several subsystems as, for example, illustrated in Figure 1.

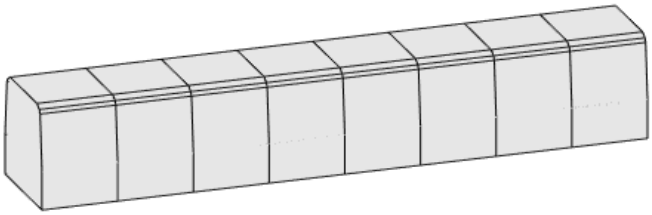

Figure 1. Subdivision of a typical train internal space.

The power balance for each subsystem is expressed as [26]

$$\omega\eta_i E_i + \sum_{j=1, j\neq i}^{n} \omega\eta_{ij} E_i - \sum_{j=1, j\neq i}^{n} \omega\eta_{ji} E_j = P_{\text{in},i}, \quad i = 1,2,3, \ldots \tag{1}$$

where $P_{\text{in},i}$ is the power input to subsystem i, E_i is the energy in the respective subsystem, ω is the angular frequency, η_{ij} are coupling loss factors between subsystems i and j ($i \neq j$) and η_i is the dissipation loss factor in subsystem i. For acoustic subsystems, expressions for the dissipation loss factor η_i in each subsystem and the coupling loss factor (CLF) η_{ij} between two subsystems are [26]

$$\eta_i = \frac{c_0 \mathrm{S}_i \alpha_i}{4\omega V_i} \tag{2}$$

$$\eta_{ij} = \frac{c_0 \mathrm{S}_{ij} \tau_{ij}}{4\omega V_i} \tag{3}$$

where c_0 is the speed of sound, S_i is the total surface area of subsystem i, α_i is its average absorption coefficient, V_i is the volume of subsystem i, $S_{ij} = S_{ji}$ is the area of the interface between cavities i and j, and τ_{ij} is the transmission coefficient of this interface. It is assumed that there is no coupling between two unconnected subsystems.

It should be noted that in a long space, such as the enclosure of the train cabin, the associated modes are undoubtedly global in character at low frequency. The assumption that there is no coupling between two unconnected subsystems may not accurately represent the acoustic behaviour in such a long space at low frequency, but according to Fahy [11] it is reasonable to assume that it is valid at sufficiently high frequencies. CLFs obtained from ESEA can allow both direct and indirect couplings [27] but this is not usual in predictive SEA. According to Craik [26], the spatial sound decay in long spaces may be overestimated when using a conventional SEA approach in which the CLFs are obtained from a transmission coefficient (as in Eq. (3)). Instead, Orrenius et al. [28] used modified CLFs, which are derived from a design formula for the energy decay in corridors in a diffuse sound field [16]. The resulting CLFs are a function of the cavity length and the absorption area and are used to force the discretized SEA formulation to fit the physics of the corridor problem. For the present application, however, it is found that the CLFs suggested by Orrenius et al. [28] do not provide an improvement in agreement with measurements compared with the conventional CLFs presented in Eq. (3). Forssén et al. [15] employed Eq. (3) to obtain the CLFs for their SEA model of a railway vehicle and found a good agreement with measurements; their subsystems were quite long and some adjustments were made to introduce sound decay in each subsystem using the formulae for corridors. In the present work, the conventional CLFs are used, but the adjustment for decay is not introduced as the length of each cavity is shorter than that in [15].

By solving Eq. (1), the stored energy in each subsystem can be obtained. Sound pressure levels in each acoustic subsystem are obtained from the stored energy as [29]:

$$L_{p,i} = 10\log_{10}\left(\frac{\rho c_0^2 E_i}{V_i} \Big/ {p_{\mathrm{ref}}}^2\right) \tag{4}$$

where p_{ref} is the reference sound pressure, 2.0×10^{-5} Pa.

3 Power input to the SEA model

This SEA model is only used to represent the interior acoustic space, unlike those in reference [14, 20] which also include the exterior noise sources and sound transmission. One-way coupling is assumed for the train floor and sidewalls. The sound transmission loss of a train body is more than 20 dB above 100 Hz [17, 20]. The power transmitted back to the outside will therefore be negligible and the one-way coupling assumption is reasonable. The input power is calculated by multiplying the sound power incident on the train floor and sidewalls by their corresponding transmission coefficients. These incident sound powers are calculated using different methods [30, 31]. They are summarised in Section 3.1 and Section 3.2. For rolling noise sources in free field the incident sound power on the roof is neglected.

3.1 Sound power incident on vehicle floor

The volume of air under the train can be represented by an enclosure limited at the sides by two open areas and any skirts, at the top by the complex geometry of the train floor and at the bottom by the sleeper/ballast surface. In a reverberant space the sound emitted by a source will consist of a direct field and a reverberant field. Usually the direct field is only significant close to the source, within the so-called reverberation distance. In the present case the distance from the sources to the train floor is only around 1 m so it is necessary to account for the direct field. The sound entering the reverberant field is that which is reflected from the surfaces; multiple reflections subsequently occur leading to the formation of the reverberant field.

In this environment the total sound power incident on the train floor (W_{f}) can be expressed as the sum of a direct (W_{dir}) and a reverberant (W_{rev}) component [32]

$$W_{\mathrm{f}} = W_{\mathrm{dir}} + W_{\mathrm{rev}} \tag{5}$$

The direct sound can be calculated by modelling the wheel, the rail and the sleepers as equivalent point sources [30, 33]. For the wheels, a point source S_q is located at the geometrical centre of the wheel [30]. The radial and axial radiation of the wheel are modelled by a monopole and a lateral dipole respectively according to their directivity [3]. The rail is instead represented by a linear array of coherent point sources. The rail vertical vibration and the sleepers are modelled by monopole sources and the rail lateral vibration is modelled by lateral dipoles according to their radiation properties [3]. It is assumed that the wheels, the rails and the

sleepers contribute incoherently to the total sound power on the train floor. The direct sound power incident on the train floor is therefore calculated by

$$W_{\mathrm{dir}} = \int_S \frac{1}{2} \mathrm{Re}(p u_z{}^*) \mathrm{d}S \tag{6}$$

where p is the sound pressure incident on the train floor and $u_z{}^*$ is the conjugate of the corresponding velocity normal to the train floor [30].

The reverberant part of the sound power can be modelled by using an SEA model. Details of the SEA model below the vehicle are elaborated in Ref. [30]. The space beneath the vehicle is subdivided into several segments, as illustrated in Figure 2.

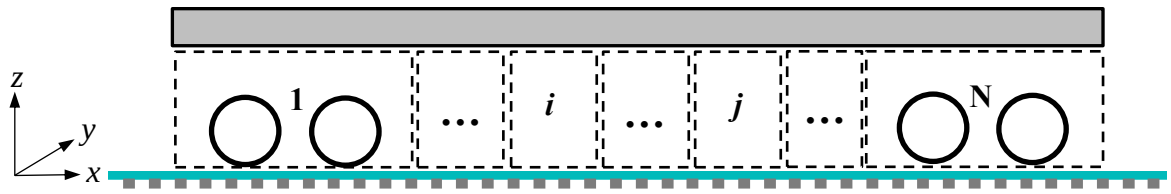

Figure 2. SEA model for reverberant sound power below the train.

The power input to the SEA system is assumed to be the sound power reflected from the direct sound incident on the train floor and the ground; it is given by incident sound power multiplied by the reflection coefficient of the boundaries, where the reflection coefficient is 1 – α, with α the absorption coefficient of the surface. The dissipation loss factors of each subsystem are determined from the absorption coefficients of the surfaces following Eq. (2). As the sides are open and the exterior domain is not included in the model, the 'absorption coefficients' of the open areas are expected to be 1. The absorption coefficient of the ballast can be obtained from measurements made in a reverberation room in [34]. The sleepers are made of concrete in most cases and their absorption coefficient can be set to be 0. The transmission coefficient between adjacent subsystems is set to be 1 to calculate the coupling loss factor in Eq. (3). The reverberant sound pressure can be found by solving the SEA model in Figure 2. The reverberant sound power incident on the train floor can be obtained by [29]

$$W_{\mathrm{rev}} = \overline{\langle {p_{\mathrm{rev}}}^2 \rangle} \frac{1}{4\rho_0 c_0} \, S \tag{7}$$

with p_{rev} being the reverberant sound pressure in each subsystem and S being the corresponding train floor area.

After the direct and reverberant sound power being calculated, they are adjusted by the source strengths of rolling noise obtained from the TWINS model [35], which is presented in [30].

3.2 Sound power incident on vehicle sides

To calculate the sound power incident on the train sidewalls, a 2.5D BE method is adopted [31]. Partially absorbing boundaries can be modelled through their surface normal impedance, which can be obtained by means of analytical or empirical models. In this case the corresponding parts of the boundaries are meshed using boundary elements. For simplicity the Delany-Bazley model for the impedance [36] is adopted in the current work to model a partially absorbing ground surface. Applying this method, the sound pressure on the train external surfaces can be obtained in the wavenumber domain. The spatial distribution of sound pressure can be calculated from applying an inverse Fourier transform.

The wheels, the rails and the sleepers are considered as separate sources in the 2.5D model and the resulting sound pressures are combined incoherently to obtain the total sound pressure distribution over the train surfaces. As in Section 3.1, the wheel is modelled by point sources: the radial component of the wheel is modelled by implementing a monopole-like source and the axial component is modelled by giving a lateral oscillation to the same fundamental source (equivalent to a dipole). A method to introduce point sources in a 2.5D model is presented in ref. [31].

The rail extends indefinitely in the x direction and can be more readily modelled in a 2.5D approach. The vibration of the rail is derived from a Timoshenko beam model on continuous support [3]. After the velocity of the rail has been obtained, the velocity of the sleepers can be derived from the ratio of the sleeper displacement to that of the rail. The 2.5D model treats the sleepers as a continuous medium in the x direction. To account for their discrete distribution and for the spacing between them, scaling factors are needed to adjust the sound power

calculated from the 2.5D model [37]. The sound power of the wheel, the rail and the sleepers obtained from the TWINS model [35] are used to adjust the 2.5D results [31].

The sound power incident on the side surfaces of the train is estimated from the sound pressure on the train sidewalls. The external sound field is not diffuse, except in a tunnel, but it is difficult to identify the incident angles associated with the sound field. Therefore, for simplicity a diffuse incident sound field is assumed. The total incident sound power per unit area for a diffuse field is half that for normal incidence for the same sound pressure. The power incident on the train external surfaces is then calculated by

$$W_{\mathrm{s}} = \frac{1}{2}\int_{S} \frac{{p_{\mathrm{tot,rms}}}^{2}}{4\rho_0 c_0}\,\mathrm{d}S \tag{8}$$

where $p_{\mathrm{tot,rms}}$ is the rms sound pressure incident on the train external surfaces due to rolling noise. The integral is performed over the areas associated with each panel based on the corresponding nodes of the BE model. The factor 1/4 is included in the integral because the sound pressure on the train external surfaces is doubled on a rigid surface whereas the incident power relates only to the incoming sound waves. The factor 1/2 outside the integral allows for the diffuse incident field assumption.

3.3 Power input to SEA model of interior noise

To calculate the interior noise, the transmission coefficients of different parts of the train structure are required. These can be derived from measurements or from predictive models. For the test case considered in this paper (see Section 4) the transmission coefficients were measured in-situ for different parts of the vehicle. Alternative approaches to calculate them include a coupled FE-BE model, as for example outlined in [38, 39]. Once the transmission coefficients are available, the power input to the interior SEA model, per subsystem, is obtained as

$$P_{\mathrm{in},i} = \sum_{j=1}^{n} I_j S_j \tau_j \tag{9}$$

where I_j, S_j and τ_j are the normal sound intensity, segment area and the corresponding transmission coefficient of the j^{th} train panel that belongs to the i^{th} subsystem of the SEA model for the train cabin. Different panels of the train structures, for example, the floor, the sidewalls, and the windows, have different transmission coefficients, so the incident sound power is dealt with separately for each panel and they are added together when calculating the input power for each subsystem.

4 Application of the framework to a metro vehicle

4.1 Predictive SEA model of the vehicle interior

The general framework outlined above is applied to predict the noise inside a Spanish metro vehicle when it was running on a surface track. Measurements were carried out with the vehicle running at 50 km/h. Figure 3 shows the interior of this metro vehicle during the field measurements [40, 41]. This carriage had four doors and five windows on each side, as shown in Figure 4, and various pieces of equipment mounted below the floor. Rolling noise was assumed to be the main noise source as other equipment was switched off where possible. The sound pressure was measured below the train floor, on the train external sides and inside the train. The sound power of the rolling noise for this train was calculated by using the TWINS model [35] with discretely supported sleepers and validated against measurements of noise at the trackside [41].

Figure 3. Overview of interior noise measurements on a running metro vehicle.

The interior surface area of the carriage is 93.7 m^2. To check whether the interior of the metro vehicle can be considered as a diffuse field, the modal overlap factor (average number of modes

within the modal half-power bandwidth) [29] was calculated and found to exceed 3 in the 160 Hz one-third octave band. Above this frequency, the sound field inside the train cabin can be considered as diffuse and the SEA method is applicable. The interior space is divided into several segments to create the SEA model. The subdivision is based on the configuration of the doors and windows, as shown in Figure 4, to allow a more straightforward calculation of the input power. Nine subsystems were created for the interior space and another two were created for the gangway at the two ends, thus giving an eleven-subsystem SEA model. There is sound power exchange between two adjacent carriages through the gangway, but they are symmetrical. Half of the gangway surfaces are therefore considered when determining the input power to this carriage, as well as the dissipation loss factor of the gangway subsystem. The length and volume of each subsystem are listed in Table 1.

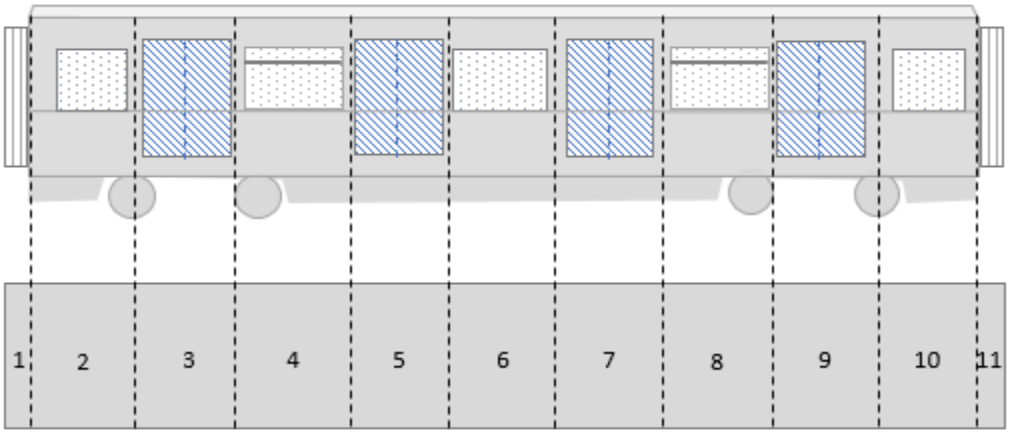

Figure 4. Division of the interior space.

Table 1. Length and volume of each subsystem.

Subsystem	T1	T2	T3	T4	T5	T6	T7	T8	T9	T10	T11
Length (m)	0.46	2	1.6	2.2	1.6	2.2	1.6	2.2	1.6	2	0.46
Volume (m^3)	2.576	11.2	8.96	12.32	8.96	12.32	8.96	12.32	8.96	11.2	2.576

It is also required that in an SEA model the modal overlap in each subsystem should be greater than 1. Subsystems T1 and T11 have the smallest volumes, and the modal overlap in these two subsystems exceeds 1 only above the 630 Hz band. For the other subsystems the modal overlap exceeds 1 from the 250 Hz band. To use the SEA method, another criterion is that in each subsystem more than five modes are present in each one-third octave band. Most subsystems have more than five acoustic modes in the 160 Hz band and above. Subsystems T1 and T11

have the smallest volumes and do not satisfy the criterion until the 250 Hz band. Considering the modal overlap factor and number of modes in each subsystem, the SEA model with this subdivision is applicable for frequency bands above 250 Hz, inclusive, apart from the small subsystems T1 and T11.

The SEA model has been created following Section 2. The values of the parameters of the SEA model, such as the dissipation and coupling loss factors, are based on the particular design of train. In the absence of partitions between adjacent subsystems, the transmission coefficient between them can be set to 1 [15]. The reverberation time is used to determine the dissipation loss factors. The interior gangways are open from one vehicle to another. However, this is unlikely to affect the reverberation time measurement significantly as all the vehicles have similar absorption. The Sabine formula therefore gives the same result whether the volume and surface area are based on a single vehicle or three vehicles. The measured absorption coefficients obtained from the reverberation time are consistent with the types of material that are present in the vehicle. To calculate the dissipation loss factors, the averaged absorption coefficients in each subsystem are determined from the measured reverberation time [41] according to the formula $\overline{\alpha} = 55.26V/(c_0 T_{60} S)$ [29], with V being the total volume of the train cabin; T_{60} the reverberation time; S the total internal absorptive surface. The same absorption coefficient is used for each subsystem. The measured reverberation time and the averaged absorption coefficients are shown in Figure 5. The absorption coefficients are quite low as the internal surfaces including the seats are mostly acoustically hard.

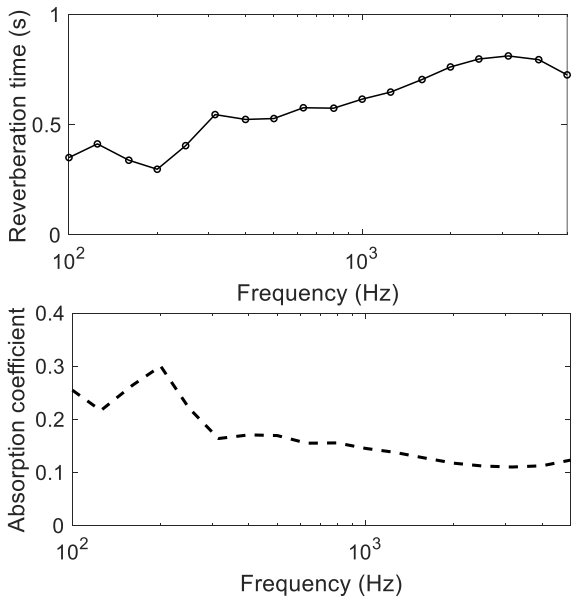

Figure 5. Measured reverberation time and absorption coefficient of the interior cabin.

4.2 Calculation of the sound incident on the train floor

The sound power incident on the train floor is calculated from the procedure described in Section 3.1. A simplified arrangement of the equipment under the train floor was taken into account when defining the SEA model of the underfloor region. This is schematically represented in Figure 6. The geometry information of each subsystem is detailed in Table 2. Direct sound is assumed only to exist on the train floor region belonging to subsystems U1, U2, U5, U7 and U8. The equipment blocks the sound from one end of the carriage from reaching the other, so when calculating the direct sound on the train floor for these subsystems due to the track, only the rail section and sleepers directly below it are considered. It is also assumed that the wheels only radiate direct sound to the floor in subsystems U2 and U7. The sound pressure impinging on the bottom of the equipment is assumed to be reflected into the corresponding subsystem and to contribute only to the reverberant sound field. An equivalent absorption coefficient of 0.2, estimated empirically, is used for the train floor and the equipment boxes. Due to the frequency dependence of the ballast absorption, this value will have some influence on the results at low frequency but negligible effect at high frequency where the ballast absorption is greater. Then, the sound power incident on the train floor can be calculated following Section 3.1.

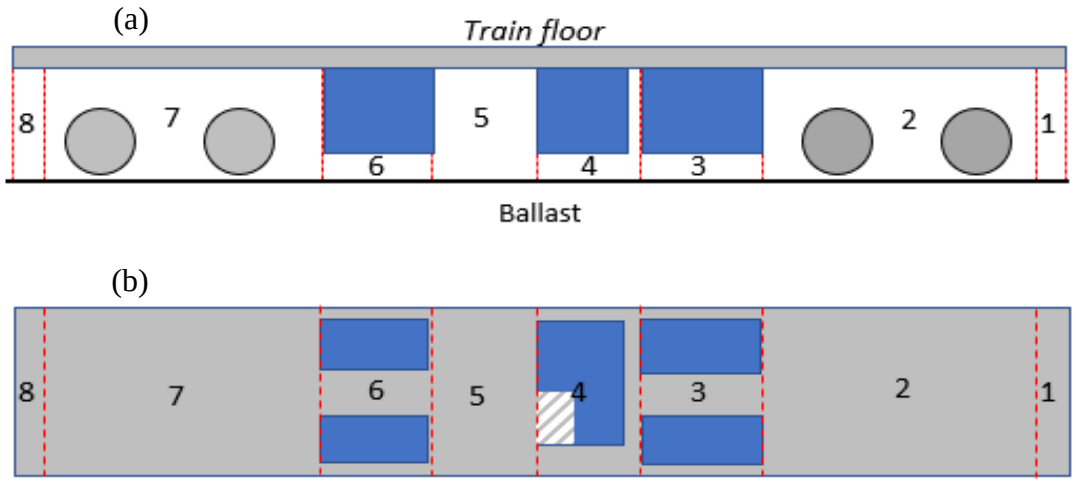

Figure 6. Subdivision of the area below the vehicle. (a) Side view, (b) top view.

Table 2. Geometry information of each subsystem for the SEA model beneath the train.

Subsystem	U1	U2	U3	U4	U5	U6	U7	U8
Length (m)	0.46	4.97	1.91	1.67	1.20	2.24	5.06	0.46
Side area (m^2)	0.49	4.74	0.74	0.67	0.48	0.89	4.84	0.49
Volume (m^3)	1.55	17.00	3.60	1.77	4.03	4.04	17.01	1.55
Interface area (m^2)	3.36	1.88	1.06	1.06	1.88	1.88	3.36	

After the sound power incident on the train floor has been calculated, it is reallocated into 11 components according to the subdivision of the interior SEA model in Figure 4 to allow the power input to this model to be determined.

4.3 Calculation of the sound incident on the train sides

The sound power incident on the train sides is calculated from the method introduced in Section 3.2. Figure 7 shows the cross-section of the 2.5D BE models used for the noise propagation from the wheel, the rail and the sleepers to the train external surfaces. The wheel contribution is modelled by using the monopole-like and the dipole-like sources, whereas the rail is modelled by its cross-section, placed 0.02 m above the ballast. The rail velocity is obtained in the wavenumber domain and is assigned to the cross-section of the rail, as outlined in Section 3.2. The ballast is replaced by a rectangular box with a thickness of 0.05 m sitting on the ground and its top surface is modelled by means of its surface normal impedance with a flow resistivity 50 $\mathrm{kPa \cdot s/m^2}$ [42]. 'CHIEF' points are used to overcome the non-uniqueness problem associated with resonances of the corresponding interior problem [43]. The train considered in this work has fairings between the bogies but these do not cover the bogie area [31], so fairings are not included when the 2.5D model is used to calculate the wheel contribution; however, they are included for the rail/sleeper contribution. The corresponding rolling noise sound power components are given in [31]. Figure 8 shows the overall sound pressure levels on the train sides due to rolling noise (two bogies below the carriage and the closest one below the adjacent carriage on each side are considered). The sound pressure distribution along the longitudinal direction of the car body shows only small differences in sound pressure levels: the sound pressure level in the middle is 2-3 dB(A) lower than at the ends, which is consistent with the results obtained by using commercial software in ref. [18].

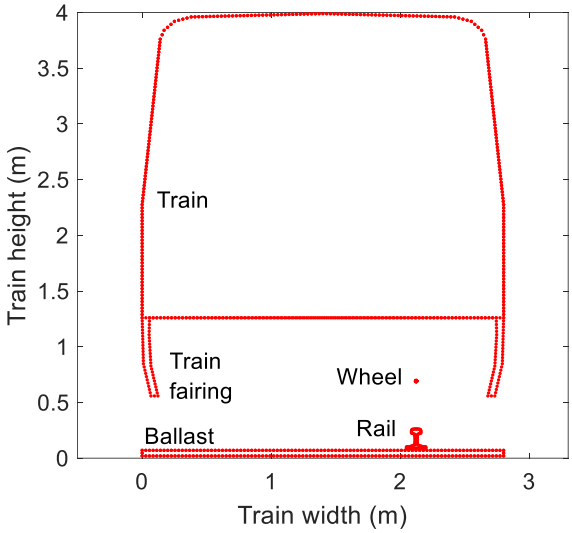

Figure 7. 2.5D models. The model for the wheel omits the fairing.

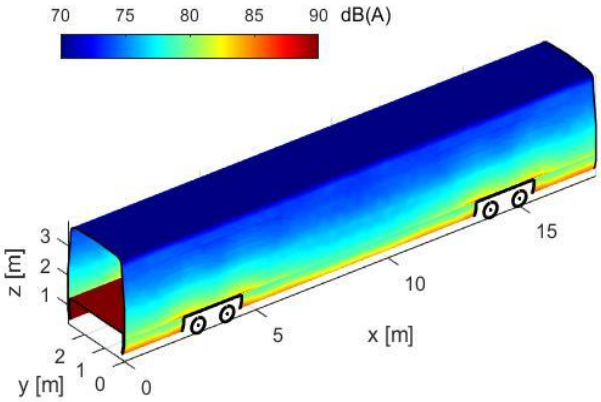

Figure 8. Sound pressure distribution on external train surfaces (four bogies were considered).

4.4 Sound power transmitted to the train cabin

During the measurement campaign [40, 41], the sound transmission coefficients of the train floor and sidewalls were measured by adopting portable sound sources inside the vehicle and a sound intensity probe to scan the outer surfaces. The incident intensity on the panels is deduced from the mean sound pressure level inside the coach using a diffuse field assumption. The transmitted intensity is measured by scanning the outer skin of the coach with the intensity probe. To match reality, the measurements should ideally be done the other way around, but this cannot be achieved in practice as an exterior sound source will excite all panels

simultaneously. By reciprocity the sound transmission coefficient of a panel is identical in both directions when mounted between two reverberation chambers, i.e. for diffuse incidence on both sides. In the present case, however, the incident sound field on the external surface is not a diffuse field. For this reason, the sound transmission coefficient is not exactly the same when measured in the reverse direction. Nevertheless, for practical reasons it is assumed that this difference in the sound transmission coefficient can be neglected. In the transmission coefficient measurement, the intensity on sections of the train floor, the doors, the side walls (aluminium part), the windows (glass part) and the gangway were measured individually, as shown in Figure 9. As explained in Section 3.3, the transmitted power (the power input to the SEA model of the vehicle interior) is then calculated from the sound powers incident on the exterior of these surfaces, multiplied by their individual measured transmission coefficients (the values of the transmission coefficients are not shown for reasons of confidentiality).

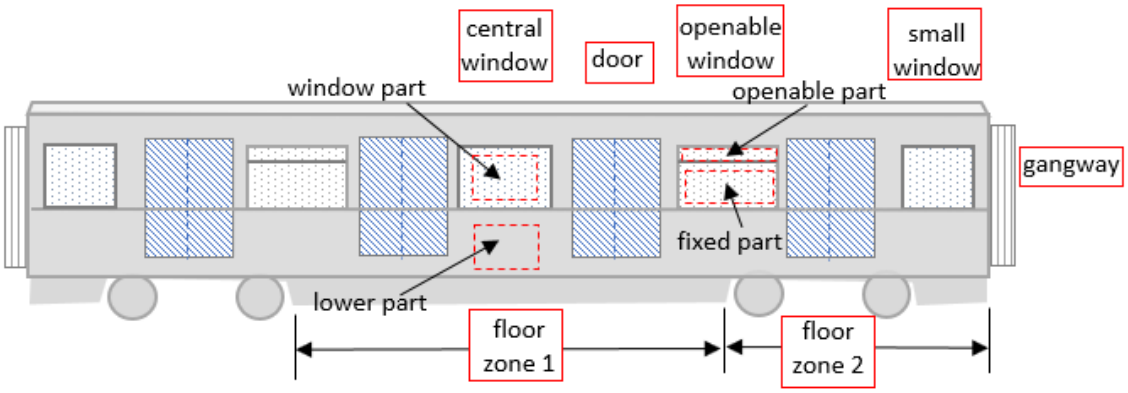

Figure 9. Definition of the panels.

The sound powers incident on the train sides (both sides), floor and gangway area are illustrated in Figure 10(a). The sound powers transmitted through the three components are compared in Figure 10(b). The largest sound power is incident on the floor. The sound powers incident on the sides and gangway are similar to each other (the gangway area is small, but it has one segment facing the ground, which can receive direct sound) and they are much lower than that incident on the floor. However, the power transmitted through the gangway is significant due to its lower sound transmission loss. The case considered in this study is a metro vehicle running on a surface track. The contribution from transmission through the train roof can therefore be neglected in the current case and it is omitted in this work.

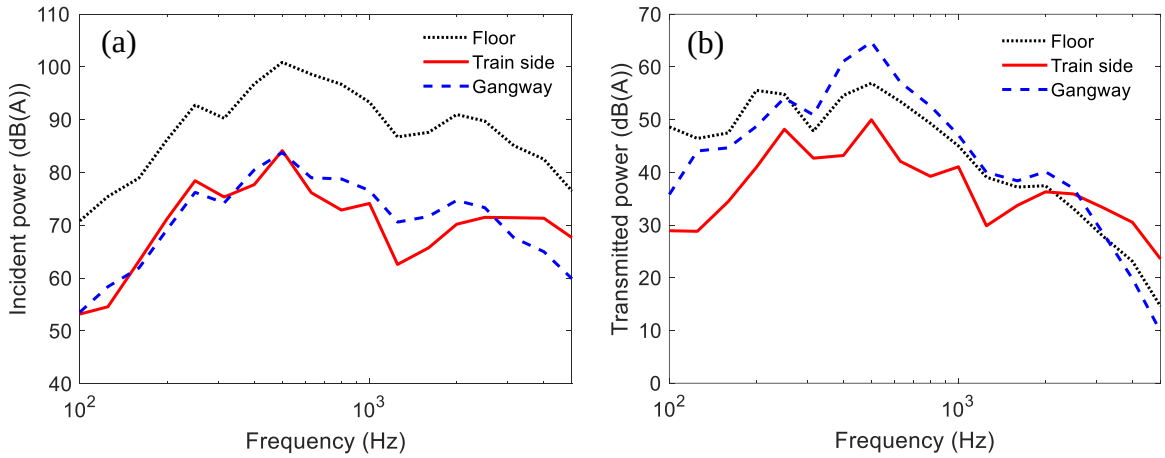

Figure 10. (a) Incident sound power, (b) transmitted sound power. Sound power levels in dB(A) re 10^{-12} W.

4.5 Sound distribution in the train cabin

The averaged sound pressure level inside the train is then calculated by using the SEA method described in Section 2. The sound pressure levels in each subsystem in the cabin are plotted in Figure 11 for different one-third octave frequency bands (actual values for the interior SPL are not shown for confidentiality reasons). The sound pressure levels at the ends of the carriage are higher than those in the middle. This can be explained by the fact that the bogies are located at the ends of the carriage, and also that the gangway has a lower sound transmission loss than other panels. The rates at which the sound pressure levels decay along the carriage vary between different frequency bands; they decay more quickly below 800 Hz than at higher frequencies. This can be explained by the low absorption coefficients at these higher frequencies (Figure 5) and also the low decay rate of the vibration of the rail. The low decay rates of the rail vibration result in a more evenly distributed incident sound power on the train external surfaces, while the low absorption coefficients in the train cabin lead to a more reverberant sound field, which results in the low decay of sound pressure levels along the train axis in the cabin at high frequency.

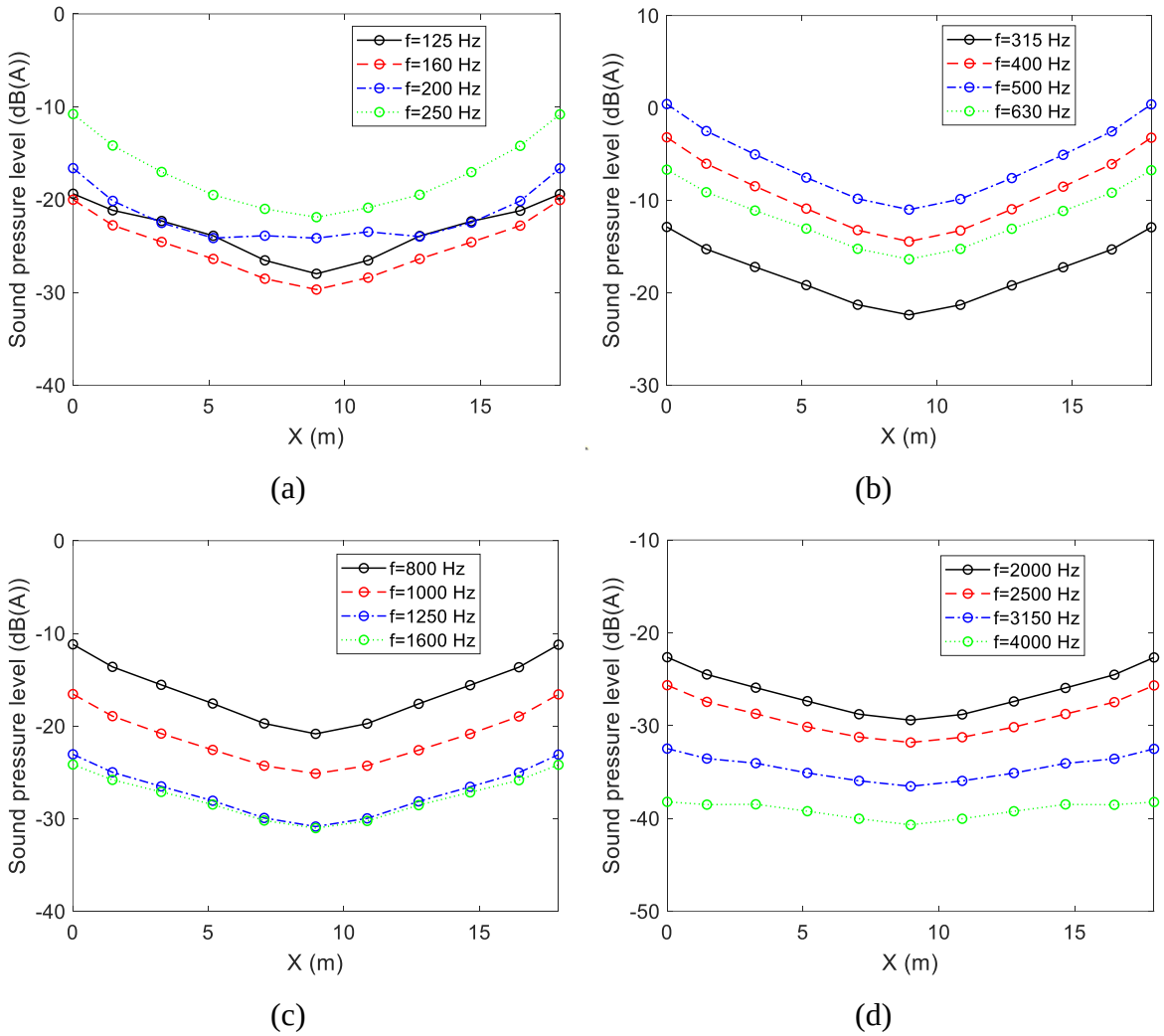

Figure 11. Sound pressure level distribution along the cabin axis, dB(A) re 2×10^{-5} Pa (values shifted for confidentiality reasons).

The sound spectra and the contributions of the three noise components, the wheel, the rail and the sleepers, to the total sound pressure at two positions inside the train cabin are illustrated in Figure 12. It is concluded that the A-weighted sound pressure levels at low and high frequency are relatively low compared with those in the mid frequency region. In terms of the contributions, it is found that the different sources have similar relative contributions at the two positions. The sound radiation from the sleepers contributes the most to the noise below 315 Hz, the rail becomes dominant between 400 Hz and 2000 Hz, and the wheel is significant above 2500 Hz.

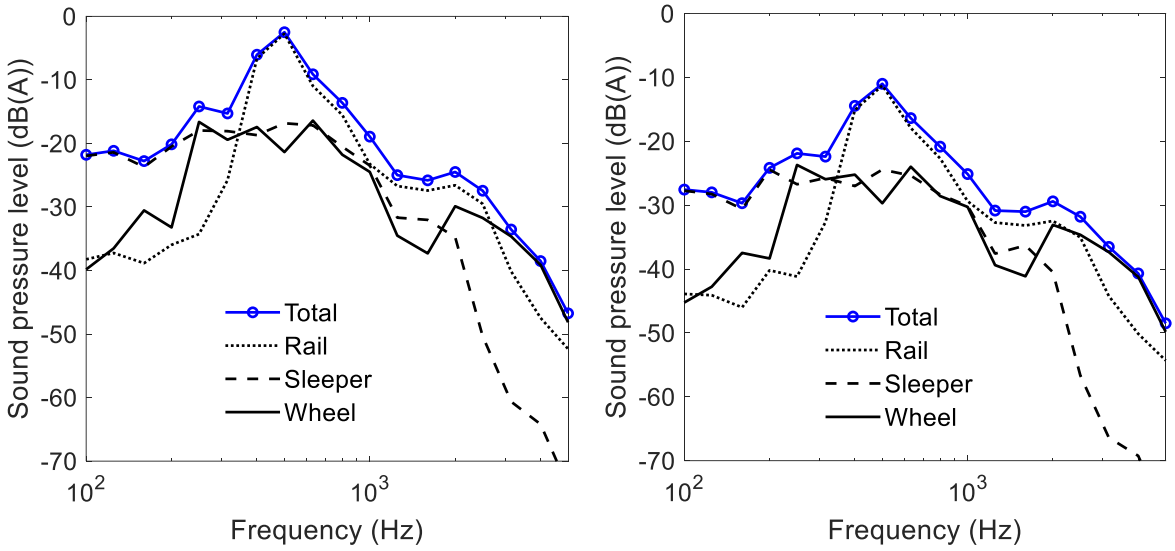

Figure 12. Sound pressure level spectra showing contributions from wheels, rails and sleepers, dB(A) re 2×10^{-5} Pa; (a) end of the carriage, (b) middle of the carriage (values shifted for confidentiality reasons).

4.6 Effect of passengers

The running tests were for an empty train. In a more realistic situation, the additional absorption of passengers should be considered. Information on the absorption of passengers is rather limited. However, Adelman-Larsen et al. [44] measured the absorption of a standing audience in a rock concert hall with a density of about 2.7 people per square metre. This is shown in Figure 13, along with absorption coefficients for a seated audience in a classical concert hall with a density of about 2 people/m^2 from Meyer et al. [45]. These absorption coefficients are defined as per floor area and, for this reason, are greater than 1 in some frequency bands. The absorption coefficients of the audiences are close to those of the train at low frequency, but they are six to eight times higher than the absorption of the train in the mid-high frequency region.

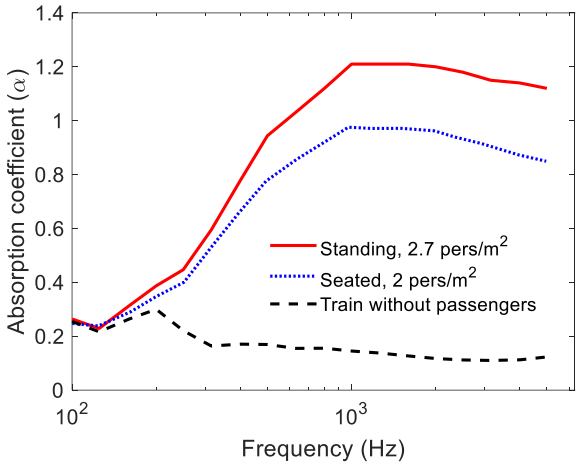

Figure 13. Absorption coefficients (per floor area) for passengers based on data for audience. Standing passengers with a density of about 2.7 people/m^2 from [44] and seated passengers with a density of 2 people/m^2 from [45], compared with the measured absorption of the train.

It can be assumed that similar absorption coefficients can be applied to the interior of a train to represent passengers. The metro vehicle in the test had about 30 seats. It is first assumed that 24 people are seated in the vehicle. Based on the density of 2 people/m^2 an area of 12 m^2 is associated with the absorption of the seated passengers. An extreme situation, representing peak time in traffic, is also considered. It is assumed that the passenger density in a fully loaded metro train is similar to that in a rock concert, i.e. about 2.7 people/m^2. This corresponds to a fully loaded metro train with 128 standing passengers in each carriage according to the train floor area. In practice, there will be complex diffraction effects between and around passengers and a reduction in the effective acoustic volume inside the train cabin, but these are ignored here.

The sound distribution along the train for these two situations is shown in Figure 14 along with the result for the empty vehicle. The passengers do not make a significant difference to the sound distribution in the cabin at low frequency because the absorption is not increased much. However, above 400 Hz the presence of passengers increases the absorption inside the train considerably, leading to a larger reduction in sound pressure level towards the middle of the vehicle.

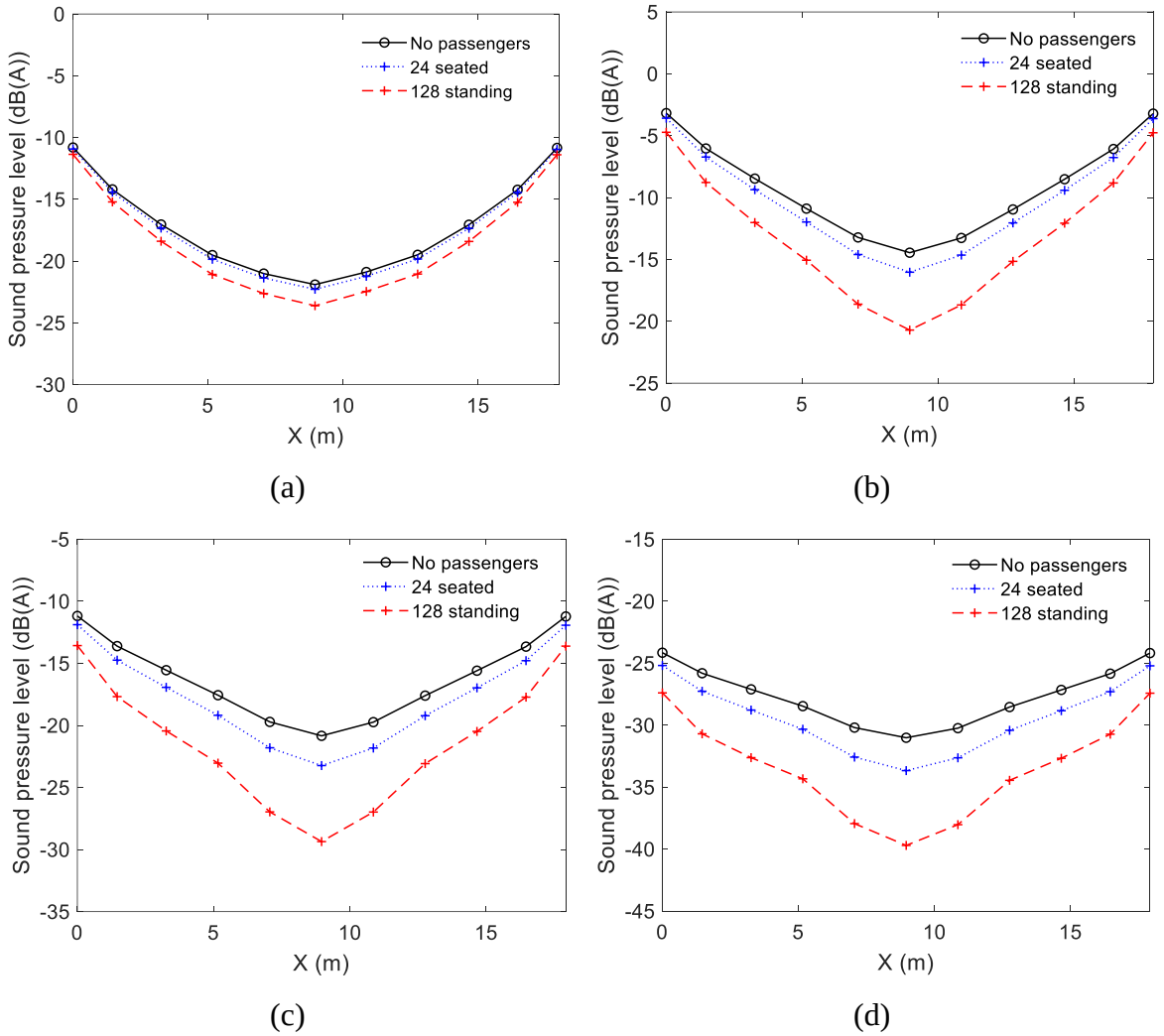

Figure 14. Sound pressure level spatial distribution under different levels of occupancy, (a) 250 Hz, (b) 400 Hz, (c) 800 Hz, (d) 1600 Hz (values shifted for confidentiality reasons).

The sound spectra in the train cabin at two locations are shown in Figure 15. The presence of the passengers provides a larger influence in the middle of the cabin than at the end. The overall sound pressure level at the end of the carriage decreases by 0.8 dB(A) for the case with 24 people seated and by 3.0 dB(A) for the fully loaded case. In the middle of the carriage, the overall sound pressure level drops by 1.7 dB(A) for the case with 24 people seated and by 6.1 dB(A) for the fully loaded case.

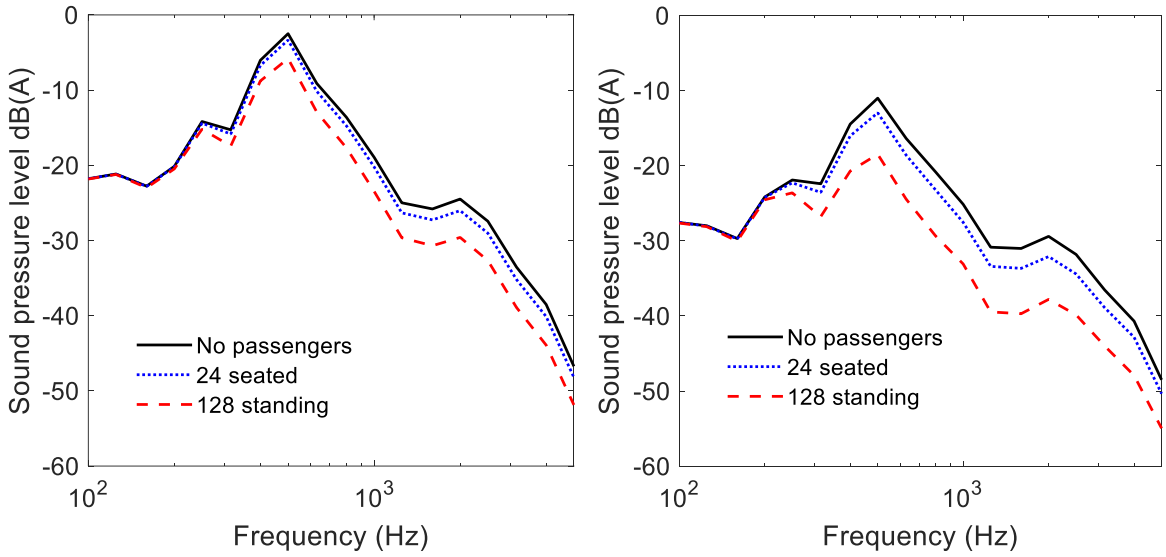

Figure 15. Sound pressure level at the (a) end of the carriage, (b) middle of the carriage (values shifted for confidentiality reasons).

5 Comparisons with measurement

5.1 Sound on the train floor

Figure 16 shows the measurement positions used for sound pressure outside the train and also inside the vehicle [40, 41]. The vehicle was runing at 50 km/h.

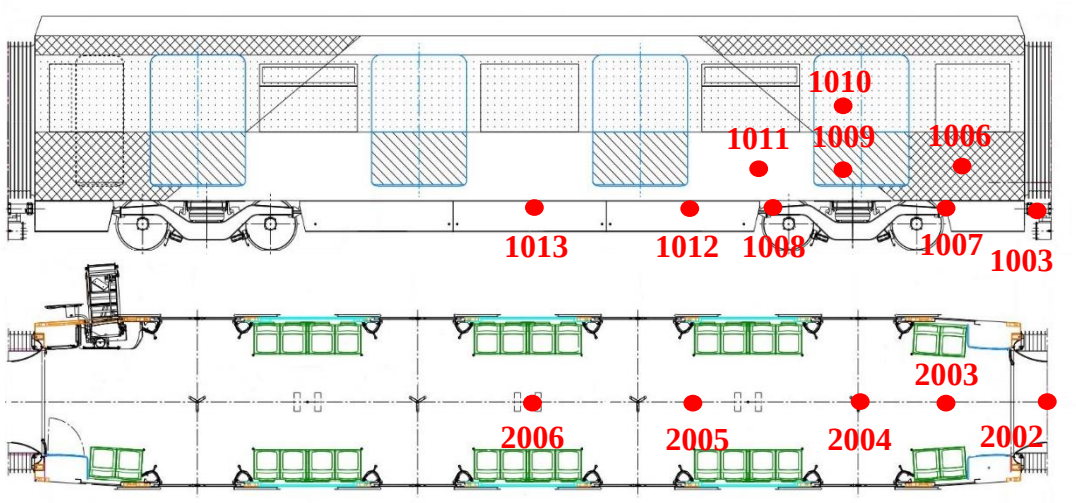

Figure 16. Experimental set-up for measuring of sound pressure outside (upper) and inside the vehicle (lower).

The sound pressure below the vehicle was measured at six microphone positions on the lower face of the train floor, as shown in Figure 16 (only five are shown, points 1003, 1007, 1008, 1012 and 1013). Details of the measurements below the vehicle are presented in ref. [30, 41]. Results are shown for two example points (point 1003 at the gangway and point 1008 nearer to the middle region of the train floor). The predictions and the field measurements of the sound pressure levels are compared in Figure 17. The sound pressure spectra obtained from the predictions and the measurements agree well. The errors of the overall sound pressure levels are between 0.2 dB to 2.9 dB among the six locations.

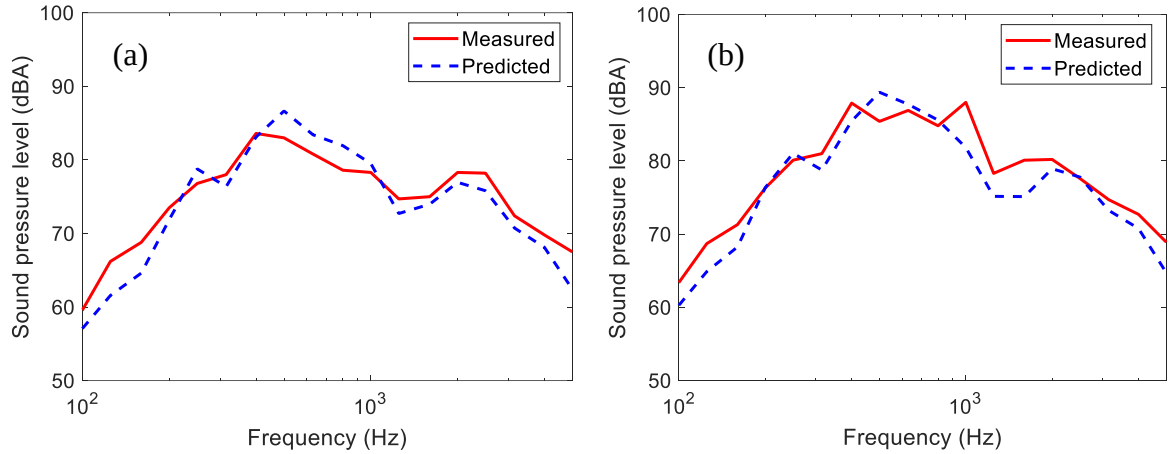

Figure 17. Comparison of predicted and measured sound pressure levels beneath the vehicle, dB(A) re 2×10^{-5} Pa; (a) at the gangway (point 1003), (b) nearer to the middle region (point 1008).

5.2 Sound on train sides

Field measurements of sound pressure on the train sides were performed. Four microphones were located on the train side above the bogie area (points 1006, 1009-1011), as shown in Figure 16. Details of the measurements are presented in ref. [31, 41]. Microphones labelled 1006, 1009, 1011 were 0.7 m above the bottom edge of the sidewall and microphone 1010 was 1.5 m above it. Sound pressure levels at two positions on the train external surfaces predicted from the 2.5D models are compared with the measurements in Figure 18. The other two positions are similar, and not shown here. The relative errors in terms of the overall sound pressure levels are less than 3 dB at these four measurement positions. The predictions capture the main trend of the sound pressure spectra compared with the measurements.

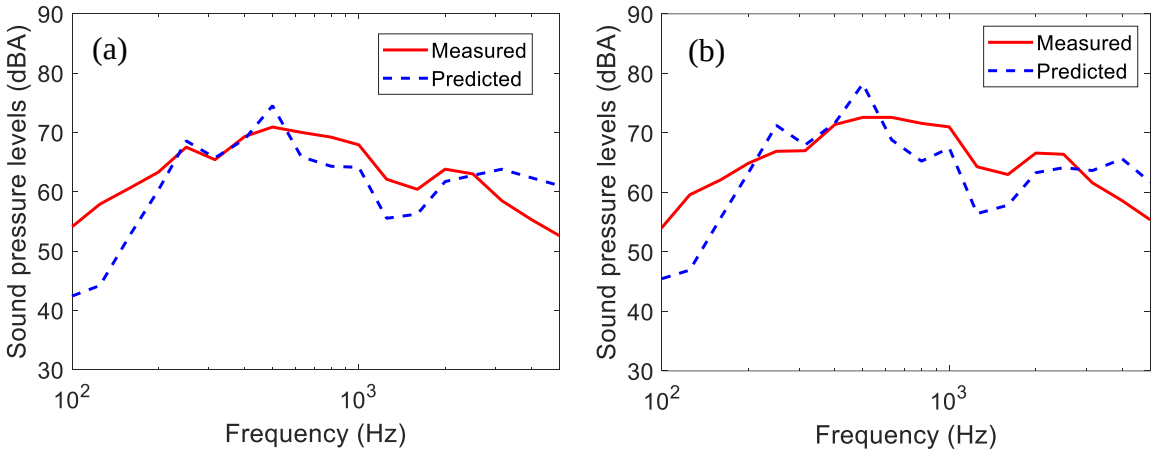

Figure 18. Comparisons between the 2.5D predictions and the measurements on a running vehicle, dB(A) re 2×10^{-5} Pa. (a) Point 1010, (b) point 1011.

5.3 Interior noise

Field measurements of sound pressure inside the train were performed. Five positions were measured on the centre line of the carriage at 1.5 m above the floor, along the train axis direction (points 2002-2006), as shown in Figure 16. The predictions of the noise inside the vehicle are compared with the measurements in Figure 19. Although the predictions only include the airborne noise component, from ref. [41] the measurements showed that the structure-borne noise is only important below 160 Hz. In Figure 19, the predicted the sound pressure levels agree well with the measurements below 1000 Hz although there is a consistent over-prediction at 500 Hz. The under-prediction found in the exterior sound pressure levels below 200 Hz, as shown in Figure 18, is not found in the interior of the carriage, because the largest part of the sound power is transmitted to the interior from the gangway region and the sound power incident on the gangway is relatively well predicted, as shown in Figure 17(a). At high frequencies, an under-prediction is found. There is a peak in the measured sound pressure levels in the 3150 Hz band at some locations, especially at position 2004. This is not present in the measured sound pressure levels beneath the train or on the train side surfaces. It is therefore believed that this is due to other interior noise sources that were not accounted for, which have caused this under-prediction at high frequency.

Apart from these disagreements, reasonable agreement is obtained in terms of overall sound pressure levels: the overall level is over-predicted by about 3 dB(A) in the gangway and about 2 dB(A) at the end of the carriage, which is possibly due to an over-prediction of the input

power to the SEA model in the 500 Hz band. The overall level in the middle of the carriage is under-predicted by about 1 dB(A).

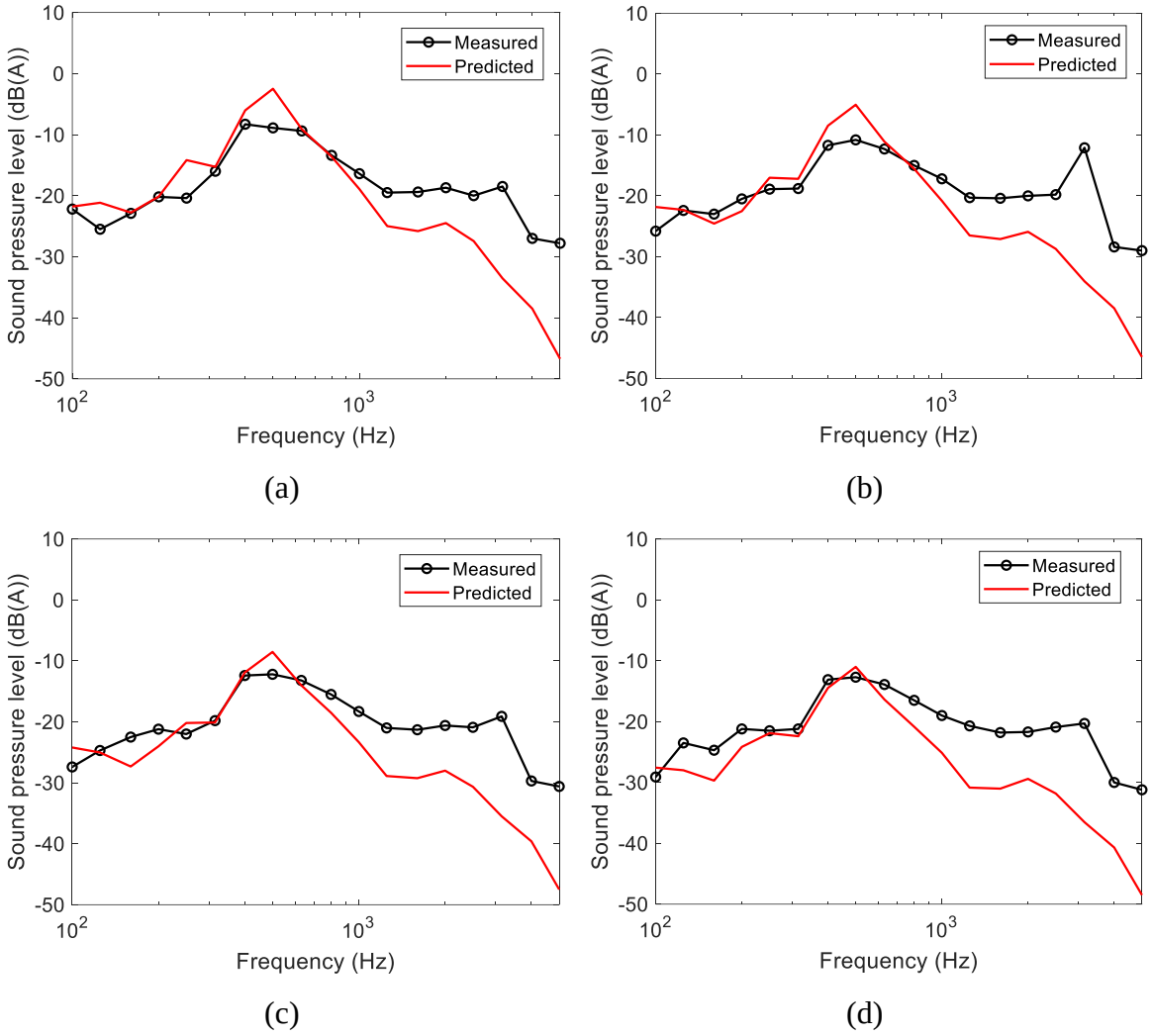

Figure 19. Comparison between predictions and measurements, (a) point 2003, (b) point 2004, (c) point 2005, (d) point 2006 (values shifted for confidentiality reasons).

Figure 20 compares the measured and predicted sound pressure distribution along the train cabin. Results are shown in two one-third octave frequency bands, 400 Hz and 800 Hz as examples, as well as the overall sound pressure distribution. There are some differences in sound pressure levels but the predictions and the measurements have similar trends. From both measurements and predictions, the interior noise distribution shows that the ends of the cabin are noisier than the middle (about 6 dB(A) difference in the measurements; about 10 dB(A) in the predictions). The sound transmission within the vehicle along the longitudinal direction of the vehicle is higher than the measured value, which is a feature of the SEA method when it is applied to long spaces [27].

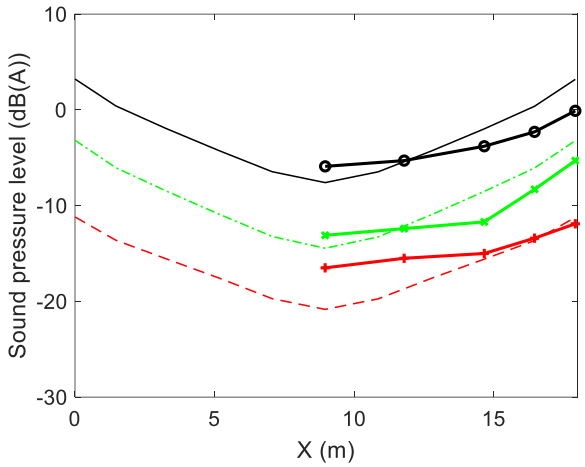

Figure 20. Comparison of sound decay along the train between predictions and measurements. -·-·-: 400 Hz, SEA; - - -: 800 Hz, SEA; ——: Overall, SEA; —×—: 400 Hz, Measured; —+—: 800 Hz, Measured; —●—: Overall, Measured (values shifted for confidentiality reasons).

In Figure 19 and Figure 20 the predicted spectra are similar to the measured ones at low frequency. Some errors appear in the 500 Hz band. In this band the rail noise is the dominant source. It has been verified by exterior sound pressure level measurements but the sound incident on the surfaces may be different (e.g. due to differences in directivity). The over-prediction of sound pressure in the 500 Hz band has also been found in Figures 17 and 18, from which it seems that the error in the exterior pressure has propagated to the interior. Besides, some differences appear at high frequency. Apart from the possibility that additional exterior and interior noise sources were present that have not been allowed for, there are other assumptions in the SEA model that might cause the discrepancies. For instance, the sound incident on the train external surfaces is calculated based on the assumption of a diffuse incident field. Also, the measured sound transmission loss is likely to be less accurate at high frequencies.

6 Discussion

In this paper, rolling noise is considered as an important example to illustrate the use of this framework to predict the airborne noise insides railway vehicles. In the field tests [40, 41], other noise sources, such as the equipment mounted below the train floor and the air conditioning and ventilation systems were switched off as far as possible. However, the same

framework can also be used to predict the contributions of other sources where present. This would require the sound power of each source, which could be obtained from measurements. They could be introduced into the model in a similar way to the wheels, i.e. as point sources, according to the procedure described in Section 3.1. The noise from the air conditioning and ventilation systems that is directly transmitted to the interior can be added to the interior SEA model as input power to its subsystems [15].

In the proposed framework, the wheels are considered as point sources. In [31] it was found that if the wheel is represented instead by multiple sources, the sound pressure on the train sides is affected by less than 0.5 dB so the point source model seems adequate. According to their radiation directivities [3], the radiation from the axial vibration of the wheel is represented by a horizontal dipole and the radiation from the radial vibration is modelled by a monopole. The directivities of the rail sources are also simplified to line monopoles or dipoles. These simplified directivities have been verified by comparison with measurements in [3] (and associated references). Although not capturing the full details of the directivity they replicate the overall trends.

The predicted sound pressure levels outside the vehicles show some disagreements with the measurements at low frequency. However, these do not affect the interior noise prediction in the current metro vehicles, because a large part of the sound power is transmitted to the interior from the gangway region (see Figure 10) and the sound power incident on the gangway is predicted relatively well (Figure 17(a)).

When calculating the sound power incident on the side surfaces of the train, for simplicity a diffuse incident sound field is assumed. The external sound field is closer to grazing incidence. The effect of this requires further investigation. The sound incident on the train floor is assumed to be the sum of the direct and reverberant sound pressure, based on the principle of noise in an enclosure. This requires the space to be sufficiently large compared with the acoustic wavelength. These models for the prediction of noise below the vehicle are shown to be valid at 315 Hz and above in [30].

The sound transmission within the vehicle predicted by the SEA model in the carriage is higher than the measured values, which is a feature of the SEA method when it is applied to long

spaces [11].The experimental SEA approach could be employed to adjust the CLFs in order to improve the accuracy [27].

Some of the results and conclusions found here may be specific to the type of vehicle and the test conditions considered. For example, in the field measurements, it is found that the largest sound power is transmitted to the interior of the metro vehicle from the gangways; the measured noise in the middle of the carriage is about 6 dB(A) lower than at the carriage ends; and the relative contributions of rolling noise components at the end and in the middle of the vehicle are similar. However, the main purpose of the field measurements was to verify the validity of the proposed framework for the prediction of the airborne noise inside railway vehicles rather than to investigate these particular features.

7 Conclusions

A framework is introduced to predict the sound field inside a railway vehicle due to rolling noise. The interior noise is predicted by using an SEA model of the vehicle cabin. The dissipation loss factors are determined from the measured reverberation time. The input power is calculated by combining measured transmission losses of the train floor and sidewalls with the sound power incident on them. The latter is determined by using a combination of an equivalent noise source model and SEA for the under-floor area and a 2.5D boundary element method for the train sides.

The calculation procedure is applied to a metro vehicle in free field. The results show that the sound power incident on the floor is about 15-20 dB higher than that on the train sides and gangway. The power incident on the sides and gangway are similar in level. For the case studied, a large proportion of the power is transmitted into the train cabin from the gangway region, due to its lower sound transmission loss. From both measurements and predictions, the interior noise distribution shows that the ends of the cabin are noisier than the middle (about 6 dB(A) difference in the measurements; about 10 dB(A) in the predictions).

Field measurements of the sound below the vehicle, on the train side surfaces and inside the train cabin were used to validate the predictions from the models. Below the vehicle, the differences in terms of overall sound pressure levels between the predictions and measurements are less than 2 dB(A) in the bogie region, and less than 2.5 dB(A) outside the bogie region. On

the train sides, the predictions and the measurements have less than 3 dB(A) difference. For the comparison inside the cabin, the differences are less than 3 dB(A). These results show that the efficient framework introduced in this paper gives adequate predictions for train interior noise. This approach could be used in railway engineering at the early design stage.

Modifying the interior dissipation loss factors will have a significant effect on the noise distribution in the train cabin. When the dissipation loss factors in each subsystem are halved or doubled, the change of sound pressure levels is smaller at the ends of the carriage and greater than 3 dB in the middle. When the train is loaded with passengers, the sound pressure levels in the middle of the train cabin will not decrease significantly at low frequency but there is considerable decrease of sound pressure level for frequencies above 400 Hz. In the fully loaded train, the overall sound pressure levels in the middle of the carriage are reduced by about 6 dB(A).

Acknowledgements

This work has been funded by the China Scholarship Council and the RUN2Rail H2020/Shift2Rail project (Grant agreement No: 777564). The contents of this publication only reflect the authors' views and the Shift2Rail Joint Undertaking is not responsible for any use that may be made of the information contained in the paper.

The authors are grateful to CAF (Construcciones Y Auxiliar de Ferrocarriles), and especially to Ainara Guiral, for assistance with information on the vehicles. The authors are also grateful to José Martínez-Casas, Javier Carballeira and Juan Giner-Navarro from UPV, Bruno Delescluse from Vibratec and Miguel A. Garralaga and José A. Chover from Metro de Madrid for their assistance with the measurements.

References

[1]. P.W. Eade, A.E.J. Hardy, Railway vehicle internal noise, Journal of Sound and Vibration 51(3) (1977) 403-415.

[2]. A.E.J. Hardy, R. Jones, Control of the noise environment for passengers in railway vehicles, Proceedings of the Institution of Mechanical Engineers, Part F: Journal of Rail and Rapid Transit 203(2) (1989) 79-85.

[3]. D. Thompson, Railway noise and vibration: mechanisms, modelling and means of control, Elsevier, Oxford, 2008.

[4]. P. Bouvet, M. Rissmann, Industrial methodologies for the prediction of interior noise inside railway vehicles: airborne and structure bone transmission, 13th International Workshop on Railway Noise, Ghent, Belgium. 2019.
[5]. F. Letourneaux, S. Guerrand, F. Poisson, Low-frequency acoustic transmission of high-speed trains: simplified vibroacoustic model, Journal of Sound and Vibration 231(3) (2000) 847-851.
[6]. H. Guo, Y.S. Wang, N.N. Liu, R.P. Yu, H. Chen, X.T. Liu, Active interior noise control for rail vehicle using a variable step-size median-LMS algorithm, Mechanical Systems and Signal Processing 109 (2018) 15-26.
[7]. L. Yan, Z. Chen, Y.F Zou, X.H He, C.Z. Cai, K.H. Yu, X.J. Zhu, Field study of the interior noise and vibration of a metro vehicle running on a viaduct: a case study in Guangzhou, International Journal of Environmental Research and Public Health 17(8) (2020) 2807.
[8]. B.K. Kim, J.G. Ih, On the reconstruction of the vibro-acoustic field over the surface enclosing an interior space using the boundary element method, The Journal of the Acoustical Society of America 100(5) (1996) 3003-3016.
[9]. P. Shorter, B. Gardner, P. Bremner, A hybrid method for full spectrum noise and vibration prediction, Journal of Computational Acoustics 11(02) (2003) 323-338.
[10]. L. Ji, X. Sheng, X. Xiao, Z. Wen, X.S Jin, A review of mid-frequency vibro-acoustic modelling for high-speed train extruded aluminium panels as well as the most recent developments in hybrid modelling techniques, Journal of Modern Transportation 23 (2015) 159-168.
[11]. F. Fahy, A note on the subdivision of a volume of air in a vehicle enclosure into sea subsystems, Journal of Sound Vibration 271 (2004) 1170-1174.
[12]. K. de Meester, L. Hermans, K. Wyckaert, N. Cuny, Experimental SEA on a highspeed train carriage. Proceedings ISMA21, Leuven, Belgium, 151-161, 1996.
[13]. B. Stegemann, Development and validation of a vibroacoustic model of a metro rail car using Statistical Energy Analysis (SEA). Thesis for the degree of Master of Science in Engineering, Chalmers University of Technology, 2002.
[14]. M. Sadri, J. Brunskog, D. Younesian, Application of a Bayesian algorithm for the Statistical Energy model updating of a railway coach, Applied Acoustics 112 (2016) 84-107.
[15]. J. Forssén, S. Tober, A.C. Corakci, A. Frid, W. Kropp, Modelling the interior sound field of a railway vehicle using statistical energy analysis, Applied Acoustics 73(4) (2012) 307-311.
[16]. T. Redmore, S. Flockton, A design formula for predicting the attenuation of sound along a long corridor. Acoust Lett. (1977) 21-24.
[17]. X. Zheng, Z. Hao, X. Wang, J. Mao, A full-spectrum analysis of high-speed train interior noise under multi-physical-field coupling excitations, Mechanical Systems and Signal Processing 75 (2016) 525-543.
[18]. Zheng, X., Dai, W., Qiu, Y., Hao, Z. Prediction and energy contribution analysis of interior noise in a high-speed train based on modified energy finite element analysis, Mechanical Systems and Signal Processing 126 (2019) 439-457.
[19]. W. Dai, X. Zheng, L. Luo, Z. Hao and Y. Qiu, Prediction of high-speed train full-spectrum interior noise using statistical vibration and acoustic energy flow, Applied Acoustics 145 (2019) 205-219.
[20]. J. Zhang, X. Xiao, X. Sheng, C. Zhang, R. Wang and X. Jin, SEA and contribution analysis for interior noise of a high-speed train, Applied Acoustics 112 (2016) 1158-170.

[21]. J. Zhang, X. Xiao, X. Sheng, D. Yao, R. Wang, An acoustic design procedure for controlling interior noise of high-speed trains, Applied Acoustics 168 (2020) 107419.
[22]. A. Bistagnino, A. Vallespín, J. Sapena, Prediction of Acoustical Wall Pressure Levels of Rolling Stock Vehicles, Notes on Numerical Fluid Mechanics & Multidisciplinary Design 126 (2015) 675-682.
[23]. T. Kohrs, K.R. Kirchner, D. Fast, Sound propagation and distribution around typical train carbody structures. in InConference Proceedings, Euronoise. 2018.
[24]. U. Orrenius, Y.Y. Pang, B. Stegeman, S. Finnveden, Acoustic modeling of extruded profiles for railway cars, in Novem, Saint Raphael, 2005.
[25]. D. Duhamel, Efficient calculation of the three-dimensional sound pressure field around a noise barrier. Journal of Sound and Vibration 197(5) (1996) 547-571.
[26]. R.J.M. Craik, Sound Transmission through Buildings using Statistical Energy Analysis, England Gower Publishing Limited, Aldershot, 1996.
[27]. H. Jang, C. Hopkins, Prediction of sound transmission in long spaces using ray tracing and experimental Statistical Energy Analysis. Applied Acoustics 130 (2018) 15-33.
[28]. U. Orrenius, R. Enblom. Acoustic optimization of car-body structures: Weight efficient setting of subsystem requirements. in Inter-noise, Den Haag, Netherlands, 2001.
[29]. F. Fahy, D. Thompson, eds. Fundamentals of Sound and Vibration, CRC Press, Boca Raton, 2016.
[30]. H. Li, D. Thompson, G. Squicciarini, X. Liu, M. Rissmann, F. D. Denia, J. Giner-Navarro, Investigation of acoustic transmission beneath a railway vehicle by using statistical energy analysis and an equivalent source model. Mechanical Systems and Signal Processing 150 (2021) 107296.
[31]. H. Li, D. Thompson, G. Squicirrini, X. Liu, M. Rissmann, F. D. Denia, J. Giner-Navarro, Using a 2.5D boundary element method to predict the noise on the train side due to rolling noise, Journal of Sound and Vibration 486 (2020) 115599.
[32]. C. J. C. Jones, D. J. Thompson, and T. P. Waters, Application of numerical models to a system of train-and track-mounted acoustic shields, International Journal of Acoustics and Vibration 6(4) (2001) 185-192.
[33]. T. Kitagawa, D.J. Thompson, The horizontal directivity of noise radiated by a rail and implications for the use of microphone arrays, Journal of Sound and Vibration 329(2) (2010) 202-220.
[34]. R. A. Broadbent, D. J. Thompson, C. J. C. Jones. The acoustic properties of railway ballast. 8th European Conference on Noise Control, Edinburgh, UK, 2009.
[35]. D. Thompson, B. Hemsworth, N. Vincent, Experimental validation of the TWINS prediction program for rolling noise, part 1: description of the model and method. Journal of Sound and Vibration 193(1) (1996) 123-135.
[36]. M. Delany, E. Bazley, Acoustical properties of fibrous absorbent materials, Applied Acoustics 3(2) (1970) 105-116.
[37]. X. Zhang, D. Thompson, E. Quaranta, G. Squicciarini, An engineering model for the prediction of the sound radiation from a railway track, Journal of Sound and Vibration 461 (2019) 114921.
[38]. C.M. Nilsson, A.N. Thite, C.J.C. Jones, D.J. Thompson, Estimation of sound transmission through extruded panels using a coupled waveguide finite element-boundary element method, Notes on Numerical Fluid Mechanics & Multidisciplinary Design 99 (2008) 306-312.
[39]. Y. Zhang, D. Thompson, G. Squicciarini, J. Ryue, X. Xiao, Z. Wen, Sound transmission loss properties of truss core extruded panels. Applied Acoustics 131 (2018) 134-153.
[40]. D. Thompson, X. Liu, H. Li, G. Xie, P. Bouvet, M. Rissmann, L. Baeza, F. Denia, J. Giner, J. Carballeira, J. Martínez, M.L. Trifiletti, Complete virtual test method for

structure-borne and airborne noise transmission, RUN2Rail Deliverable 4.2. March 2019 (www.run2rail.eu).
[41]. P. Bouvet, M. Rissmann, D. Thompson, X. Liu, H. Li, G. Squicciarini, G. Xie, Validation of complete virtual test method for structure-borne and airborne noise transmission. RUN2Rail Deliverable 4.3, August 2019 (www.run2rail.eu).
[42]. X. Zhang, Modelling of track sound radiation, PhD thesis, the University of Southampton, UK, 2016.
[43]. H.A. Schenck, Improved integral formulation for acoustic radiation problems, The Journal of the Acoustical Society of America 44(1) (1968) 41-58.
[44]. N.W. Adelman-Larsen, E.R. Thompson, A.C. Gade, Suitable reverberation times for halls for rock and pop music, The Journal of the Acoustical Society of America 127(1) (2010) 247-255.
[45]. E. Meyer, D. Kunstmann, H. Kuttruff, Über einige Messungen zur Schallabsorption von Publikum, Acta Acustica united with Acustica 14(2) (1964) 119-124.